Mon. Not. R. astr. Soc. (1969) **144**, 41–54.

SOLID HYDROGEN COATED GRAPHITE PARTICLES IN THE INTERSTELLAR MEDIUM—I

N. C. Wickramasinghe and K. S. Krishna Swamy

(Received 1968 November 25)

SUMMARY

Solid hydrogen coated graphite particles may be expelled from regions of star-formation into the general interstellar medium. The solid para-hydrogen mantles, which contain a small proportion of ortho-H_2 could be stable against evaporation in the general interstellar radiation field. They are also stable against physical and chemical sputtering in H I regions. Extinction efficiencies are calculated for solid hydrogen particles and for graphite particles with solid hydrogen mantles. Graphite core–solid hydrogen grains are capable of producing excellent agreement with the interstellar extinction observations from 20 000–1100 Å. The graphite core radius may be in the range $r_0 = 0{\cdot}04$–$0{\cdot}06\ \mu$ and the solid hydrogen mantle radius in the range $r = 0{\cdot}15$–$0{\cdot}25\ \mu$. The albedo and phase function of these particles are consistent with the requirements imposed by the diffuse galactic light.

1. INTRODUCTION

It has recently been argued (**1**), (**2**) that solid hydrogen mantles may be accreted by graphite grains within dense interstellar clouds. At gas densities $\sim 10^3$–$10^4\ \mathrm{cm}^{-3}$, $2\mathrm{H} \rightarrow \mathrm{H}_2$ recombination on grain surfaces occurs if the grain temperature $T_g < 7\ ^\circ\mathrm{K}$ (**2**). Subsequent condensation onto the grains takes place if the partial pressure of H_2 exceeds the vapour pressure of solid hydrogen at the temperature of the grain. The critical condition at molecular densities $\sim 10^3$–$10^4\ \mathrm{cm}^{-3}$ is that T_g is less than $\sim 3{\cdot}4\ ^\circ\mathrm{K}$ (**2**), (**3**).

Several dark clouds are known (**4**), (**5**) to be anomalously deficient in neutral hydrogen as indicated by the strength of the 21-cm line. From an analysis of this data it could be argued that solid hydrogen may have condensed on the grains if the optical depth at visible wavelengths exceeds 3 or 4 mag. (**2**). Many of these objects and also Bok's globules (**40**) do indeed have optical extinctions exceeding 7 or 8 mag. The conditions therefore seem appropriate for the formation of solid hydrogen mantles.

The lack of detectable H II regions in young stellar associations such as Cygnus II has been interpreted by Wickramasinghe & Reddish (**1**) to imply that solid H_2 condensed on the grains prior to extensive star formation within the nebula. It would appear reasonable to suppose that a significant fraction of the hydrogen coated grains are injected into the interstellar medium after star-formation has taken place. The fragmentation of individual protostar clouds into central stellar condensations and circumstellar shells, as the observations indicate (**6**), would seem to support the view that a considerable quantity of hydrogen coated grains are blown out of the contracting stars. It is probable that such a process is associated

with the transport of angular momentum out of the central stellar condensations (**7**). Some of these grains may reach the outer regions of the nebula and even be expelled by radiation pressure into the general interstellar medium.

The maximum size to which a hydrogen mantle can grow in a condensing region is determined by the graphite grain to hydrogen ratio n_g/n_H. For a spherical grain, the maximum radius r is given by

$$r \cong \left[\frac{m_H(n_H/n_g)}{\frac{4}{3}\pi s}\right]^{1/3} \tag{1}$$

where s is the density of solid H_2, $\sim 0{\cdot}1$ g cm^{-3}. With $n_g/n_H \approx 10^{-12}$, we get $r \approx 1{\cdot}6\mu$; with $n_g/n_H \approx 10^{-10}$ we have $r \cong 0{\cdot}3\mu$. The mean radius of grains reaching the interstellar medium is uncertain on account of uncertainties in the n_g/n_H ratio as well as in the likelihood of destructive effects being associated with the ejection processes. In the present paper we shall leave r as a free parameter to be determined by requiring a match with the interstellar extinction observations.

In accordance with our earlier remarks we assume that the formation of solid hydrogen mantles on graphite grains is associated with star formation. Suppose that an increase in the smoothed out stellar mass density by $\delta\rho_{stars}$ is accompanied by the release into the interstellar medium of a mass density increment of solid hydrogen mantles

$$\delta\rho_{\text{solid } H_2} = \alpha\delta\rho_{stars} \tag{2}$$

where α is a number less than unity. Thus we have

$$\frac{d\rho_{\text{solid } H_2}}{dt} \cong \alpha \cdot \frac{d\rho_{stars}}{dt}. \tag{3}$$

It has been argued by Reddish (**8**) (see also (**7**)) that the rate of star formation within the local group of galaxies is proportional to the average mass density of the interstellar gas:

$$\frac{d\rho_{stars}}{dt} \cong 1{\cdot}3 \times 10^{-17}\ \rho_{gas}. \tag{4}$$

From equations (3) and (4) we have

$$\frac{d\rho_{\text{solid } H_2}}{dt} \cong 1{\cdot}3 \times 10^{-17}\ \alpha\rho_{gas}. \tag{5}$$

With $\rho_{gas} \approx 3 \times 10^{-24}$ g cm^{-3} and an estimated lifetime of a solid hydrogen mantle of $\sim 3 \times 10^7$ yr (see Section 2), the equilibrium density of interstellar solid H_2 is

$$\rho_{\text{solid } H_2} \approx \alpha \cdot 4 \times 10^{-26} \text{ g cm}^{-3}.$$

If $\alpha \approx 0{\cdot}25$, that is 25 per cent of the mass of protostar associations is ejected in the form of solid H_2, we obtain an equilibrium mass density

$$\rho_{\text{solid } H_2} \approx 10^{-26} \text{ g cm}^{-3}.$$

Such a density of solid H_2 in the form of particles of radii $\sim 10^{-5}$ cm could contribute appreciably to the observed interstellar extinction.

2. STABILITY OF SOLID H_2 MANTLES IN H I REGIONS

It was implied throughout the preceding discussion that the condensation of solid H_2 onto graphite particles could take place only in the interiors of dense clouds where there is some shielding from the general interstellar radiation field. Once formed, however, the solid hydrogen mantles could be quite stable even in an unattenuated interstellar radiation field. The requirement is that the crystal possesses optically active transitions at frequencies ~ 10 cm^{-1}. It has been argued by Hayakawa (**9**) that such impurity levels could arise because of the interaction of low energy cosmic rays with the solid hydrogen. The oscillation of weakly bound impurity atoms in the crystal lattice is also expected to take place at such frequencies (**10**).

In molecular hydrogen the nuclear spins may be parallel ($S = 1$, ortho-hydrogen) or anti-parallel ($S = 0$, para-hydrogen). The energy difference between these states is ~ 339 cal/mole. The rotational energy levels accessible to the ortho-molecule corresponds to $J = 1, 3, 5, \ldots$ and those for the paramolecule are $J = 0, 2, 4, \ldots$. At temperatures exceeding ~ 100°K the equilibrium concentration of para-hydrogen in an H_2 gas is ~ 30 per cent. As the temperature is lowered the para-form becomes increasingly stable, and at ~ 30°K, the equilibrium para-concentration exceeds 90 per cent. If the hydrogen mantles froze out of a H_2 gas at 3 °K, the crystal will be close to 100 per cent para-hydrogen. The situation in our case, however, is that the mantles grow out of a gas at a considerably higher temperature containing an appreciable ortho-concentration. If the ortho-to-para transition is not completely achieved at the grain's surface, it is reasonable to suppose that an ortho-concentration of a few per cent becomes frozen into the solid mantles. Sears and van Kranendonk (**11**) have argued that for ortho-concentrations $\gtrsim 2$ per cent in para-hydrogen crystals pairs of ortho molecules interact through quadrupole–quadrupole interactions and the $v = 1$, $J = 1$ levels are split by 6 cm^{-1}. According to van Kranendonk (**12**) the same splitting, 6 cm^{-1}, occurs for the ground vibrational state $v = 0$, $J = 1$. Even though the oscillator strength of the individual transitions may be low, a sufficient number of ortho-molecules could exist for $Q_{abs} \approx 1$ to be attained at ~ 6 cm^{-1}. Thus the required transitions at $\nu \approx 10$ cm^{-1} may occur quite naturally because of ortho impurities in para-hydrogen crystals.

A solid hydrogen grain at ~ 3 °K would be in equilibrium with an ambient H_2 gas of density $\sim 10^{-2}$ cm^{-3} and temperature ~ 100 °K (**3**, Table 2, $L \sim 300$ cal/mole*). Accretion would take place if the ambient molecular hydrogen density exceeds $\sim 10^{-2}$ cm^{-3}. If the ambient H_2 density in the interstellar medium is equal to this value the grain will not evaporate. If the H_2 density is less than $\sim 10^{-2}$ cm^{-3} the grain will evaporate in a timescale of $\sim 10^8$ years; as we shall see later other destructive processes are also operative over timescales $< 10^8$ years.

There is some evidence (**39**) to suggest that solid H_2 surfaces may be quite inefficient in catalysing the H_2 recombination through physical adsorption processes. If this were so, the neutral hydrogen gas in the general interstellar medium may not easily be deposited on to already existing solid H_2 particles.

* If the effect of impurities is neglected L may be somewhat lower. The arguments in this paragraph would still be valid if the grain takes up a lower temperature say $T_g \sim 2{\cdot}7$ °K. Such a temperature is indeed possible if the crystal possesses transitions at ~ 6 cm^{-1} which we have discussed.

In spite of the rather weak crystal binding of H_2, ~ 300 cal/mole, it is likely that solid hydrogen grains are stable against both reactive and physical sputtering in H I regions. For an H I region with gas temperature $T_{gas} \sim 100\,°K$, the gas atoms impinging on grains have energies $\sim 10^{-2}$ eV. Although the binding energy of H_2 in its crystal is closely similar to this, $L \sim 1{\cdot}3 \times 10^{-2}$ eV, the threshold for physical sputtering is expected to be considerably higher. A crude estimate of the threshold energy $V_{0.25}$ to produce a 25 per cent sputtering yield is

$$V_{0.25} \cong 11 \frac{(m_1+m_2)^2}{4m_1m_2} L \text{ eV} \tag{6}$$

where m_1 is the mass of the impinging ion and m_2 is the mass of an H_2 molecule (see Lynds & Wickramasinghe (**13**)). This is probably an upper limit to the actual threshold energy. For the case of either H or He atoms impinging on solid H_2 the sputtering threshold given by equation (6) is

$$V_{0.25} \cong 0{\cdot}16 \text{ eV} \tag{7}$$

much higher than the average kinetic energy of gas atoms in an H I region.

For the case of reactive sputtering (e.g. Ref. (**14**)) detailed chemical reactions must be considered. The best candidates for the destruction of solid H_2 grains are reactions with O and C:

$$\begin{aligned} O + H_2 + \Delta_1 &\rightarrow OH + H \\ C + H_2 + \Delta_2 &\rightarrow CH + H \\ C^+ + H_2 + \Delta_3 &\rightarrow CH^+ + H. \end{aligned} \tag{8}$$

The endothermicities in these reactions are $\Delta_1 \cong 0{\cdot}71$ eV, $\Delta_2 \cong 1{\cdot}0$ eV, $\Delta_3 \cong 0{\cdot}77$ eV and typical activation energies are in the range 0·2–0·3 eV. The fraction of collisions which lead to reactions, and therefore to sputterings, involve exponentials in T which are steeper than

$$\exp(-4000/T). \tag{9}$$

In H I regions with $T \leqslant 100\,°K$, the reaction rates of equation (8) are therefore completely negligible. In cloud–cloud collisions where $T \geqslant 1000\,°K$, destruction of the solid H_2 grains would readily take place. The life time of a solid hydrogen mantle is thus the mean cloud–cloud collision time $\sim 10^7$ years.

3. REFRACTIVE INDEX OF SOLID HYDROGEN

Extensive measurements of the dielectric constant K of liquid para-hydrogen as a function of the mass density ρ have been published by Stewart (**17**). Since the refractive index is related to K by $K = n^2$ we thus have

$$n = n(\rho)$$

available for liquid para-hydrogen. This function is plotted in Fig. 1.

Although no published data is available on the refractive index of solid para-hydrogen, its average value is unlikely to be significantly different from that appropriate for the liquid with the same mass density. The molar volume of the solid at $\sim 3\,°K$ is $\sim 22{\cdot}5$ cm^3/mol (**18**) so that the mass density is $\rho \approx 0{\cdot}089$ g cm^{-3}. At this

value of ρ the liquid refractive index (Fig. 1) is $\sim 1 \cdot 1$. The average refractive index of solid hydrogen is therefore likely to be close to $1 \cdot 1$, somewhat larger than the value $n = 1 \cdot 05$ which was previously used (**32**).

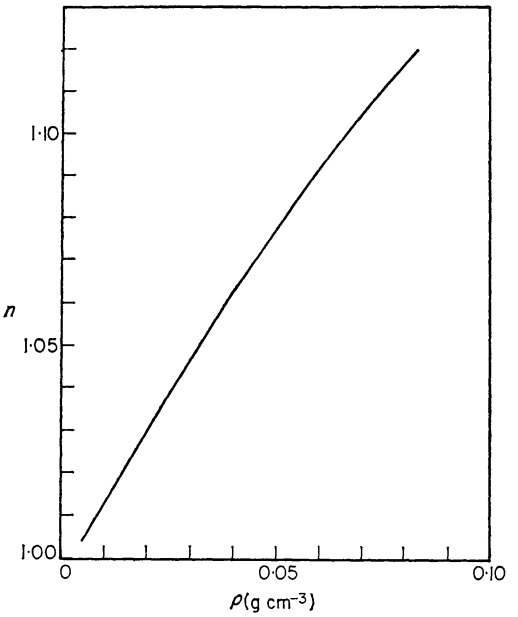

FIG. 1. *Refractive index of liquid para-hydrogen as a function of density.*

On account of uncertainties in the precise value of this quantity we shall present calculations in the subsequent sections for two typical cases: $n \cong 1 \cdot 1$, $1 \cdot 05$. It will turn out that there is no significant difference between these cases from the point of view of fitting the extinction observations. Nor are our results in this respect sensitive to the precise value of the refractive index n as long as it is in the general range $\sim 1 \cdot 13$–$1 \cdot 03$. The distinguishing feature of solid hydrogen is that it has a refractive index closer to unity than for most other solid materials.

Pure solid hydrogen is a perfect dielectric with zero absorptive index. The presence of impurities, or of radiation damage could give rise to a small absorptive index typically in the range $0 \cdot 01$–$0 \cdot 05$. In the following sections we discuss results of extinction calculations for spherical solid H_2 particles and for graphite particles covered with spherical solid hydrogen mantles. The refractive index measurements of Taft & Phillipp (**19**), (**20**) are adopted for the graphite cores. For solid hydrogen we consider several cases:

$$m = 1 \cdot 05 - ik \tag{10}$$

$$m = 1 \cdot 1 - ik \tag{11}$$

with $k = 0$, $0 \cdot 01$, $0 \cdot 02$, $0 \cdot 05$.

The real part of the refractive index, n, is expected to be almost completely wavelength independent. The value of k may decrease slightly from the infrared into the ultra-violet, but this effect is unlikely to produce a significant modification to the calculated extinction efficiencies. The dissociation continuum of H_2 starts at $\lambda < \sim 900$ Å. Thus strong absorption effects of the type discussed for ice particles (**27**), (**28**) would not arise until $\lambda < 1000$ Å. We thus consider the assumption of a constant complex refractive index for solid hydrogen to be a reasonable one for the present purposes.

4. EXTINCTION EFFICIENCIES FOR SINGLE SOLID HYDROGEN PARTICLES

The extinction efficiency Q_{ext} of a spherical solid hydrogen particle of radius a may be calculated from the Mie formulae as a function of $x = 2\pi a/\lambda$, where λ is the wavelength. For the case $n = 1{\cdot}05$ the $Q_{ext}(x)$ curves are plotted in Fig. 2; the three curves correspond to $k = 0$ (pure dielectric), and $k = 0{\cdot}01$, $k = 0{\cdot}05$. Similar curves for $n = 1{\cdot}1$ are plotted in Fig. 3.

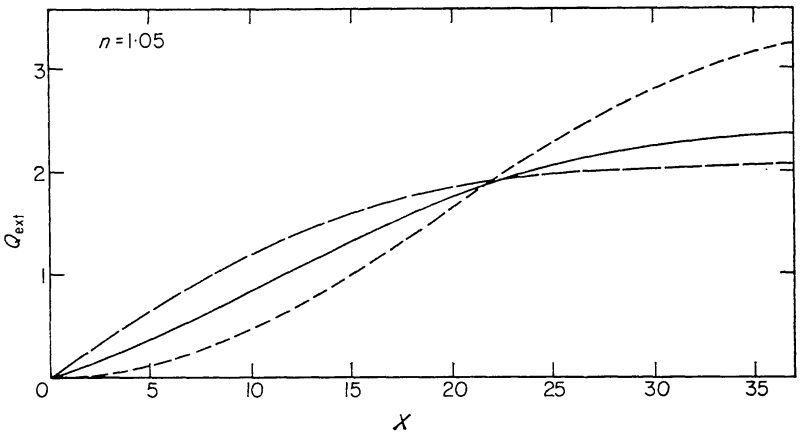

FIG. 2. *Extinction efficiencies of spherical hydrogen particles as a function of* $x = 2\pi a/\lambda$; *dashed curve continuous curve and long dashed curve are respectively for the cases* $k = 0{\cdot}0$, $0{\cdot}02$ *and* $0{\cdot}05$ *respectively.*

A feature common to all the curves in Figs 2 and 3 is that they are linear ($Q_{ext} \propto x$) over substantial intervals in x. In this respect they differ markedly from the Q_{ext} curves for larger values of n which exhibit linear segments only for rather limited ranges of x. Towards the infra-red ($x \to 0$) the shapes of the extinction curves depend critically on the value of the absorptive index. It is seen that the larger k values give rise to more linear curves as $x \to 0$.

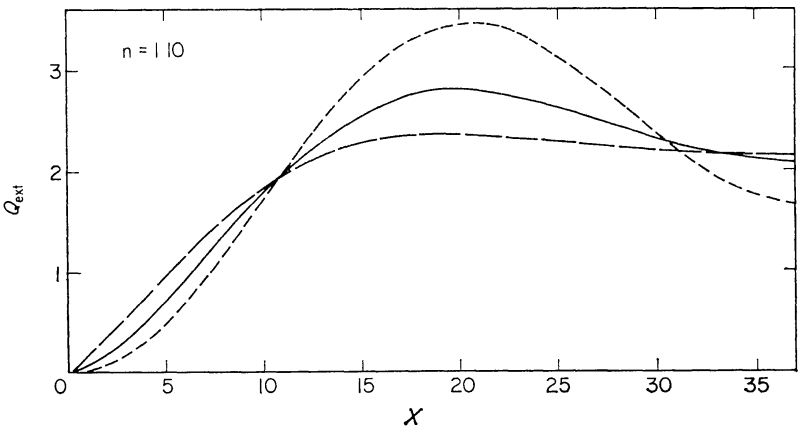

FIG. 3. *Extinction efficiencies for* $n = 1{\cdot}10$. *All the curves have the same meaning as Fig. 2.*

5. THE INTERSTELLAR EXTINCTION CURVE

The wavelength dependence of the observed interstellar extinction is usually regarded as the most straight-forward observational test of grain models. The sensitivity of this test has been much enhanced by the rocket ultra-violet observations of Boggess & Borgman (**21**), Stecher (**22**) and Bless *et al.* (**23**) which extended the wavelength base of the extinction curve up to ~ 1100 Å. In the visible spectral region accurate spectrophotometric measurements of Nandy (**24**), (**25**) have established the precise shape of the extinction curve. The interstellar extinction appears to be strictly linear (with $1/\lambda$) in the wavelength range 9000 Å–4300 Å for all regions studied by Nandy. Small, but significant regional variations have been found in the near ultra-violet (**24**), (**25**).

Dirty ice particles would appear to be quite unlikely according to the present state of the observational data (**26**), (**13**). While graphite particles are able to fit the data up to ~ 2400 Å, no agreement seems possible further in the ultra-violet. For ice-coated graphite grains general agreement with the extinction curve extends to $\lambda \sim 1500$ Å (**26**). The agreement cannot be regarded as perfect, however, if one takes into account the slight hump in the observational curve at 2400 Å reported by Stecher (**22**). The extinction curves for ice-coated graphite particles do not reproduce this hump. It has already been pointed out (**26**) that the central wavelength of this hump corresponds to the transition between π-electrons and the conduction band in graphite. The occurrence of such a hump, if it is confirmed by future experiments, would be the most definitive proof of a graphite component to the grains.

The fit for the composite graphite–ice particles is somewhat worsened if one includes the effect of the dissociation continuum of H_2O (**27**), (**28**) which introduces a large absorptive component to the complex refractive index for $\lambda < 1800$ Å. The resulting extinction curves fall somewhat short of the observations in the furthest ultra-violet. Although the extinction observations cannot be regarded as ruling out the graphite–ice grains, it is becoming evident that this model is not entirely satisfactory.

Recent attempts to measure the strength of the $3 \cdot 1\ \mu$ ice band in highly reddened stars (**29**), (**30**) would seem to indicate that very little ice is present in the grains. The strength of the ice band predicted (**31**) for graphite core–ice mantle grains appears to be somewhat greater than the upper limits set by these preliminary observations.

6. EXTINCTION CURVES FOR GRAPHITE CORE–SOLID HYDROGEN MANTLE GRAINS

The results of preliminary extinction calculations for graphite core–solid H_2 mantle grains were recently reported by Wickramasinghe & Nandy (**32**). Good fits to the observations were shown possible for a wide range of core and mantle radii throughout the visible and ultra-violet spectral regions.

The earlier calculations (**32**) were limited to the case of pure dielectric mantles of refractive index $m = 1 \cdot 05$. In the present section we present more general results, considering two refractive indices $n = 1 \cdot 05$, $1 \cdot 10$ for the solid H_2 and including the effect of a small absorptive index. The graphite refractive index was taken from the measurements of Taft & Phillip (**20**).

The extinction efficiencies $Q_{\text{ext}}(\lambda)$ for graphite core–solid H_2 grains were calculated from the Güttler formulae (see (**26**)) for various values of core radii r_0 and mantle radii r. A normalized extinction F_λ was calculated for each case according to the expression:

$$\left.\begin{aligned} F_\lambda &= 0{\cdot}5\,\frac{Q_{\text{ext}}(\lambda)-Q_{\text{ext}}(\lambda_0)}{Q_{\text{ext}}(\lambda_1)-Q_{\text{ext}}(\lambda_0)} \\ \lambda_0^{-1} &= 1{\cdot}80\ \mu^{-1};\ \lambda_1^{-1} = 2{\cdot}24\ \mu^{-1} \end{aligned}\right\}. \qquad (12)$$

For comparison with the theoretical curves the observational data (**21**)–(**24**) were also normalized according to the same relation.

In Fig. 4 we have plotted the normalized extinction for a graphite core of radius $r_0 = 0{\cdot}05\ \mu$ surrounded by solid hydrogen mantles of outer radii $r = 0{\cdot}17\ \mu$. The upper set of curves refer to a refractive index $n = 1{\cdot}1$ and the lower set to $n = 1{\cdot}05$; curves 1, 2, 3 represent respectively the cases for which the absorptive index $k = 0{\cdot}05, 0{\cdot}02, 0{\cdot}0$. The points are the observations in the visible and infra-red of Nandy (**24**) and Johnson (**33**) for the Cygnus region. It is evident from Fig. 4 that an absorptive index $k \cong 0{\cdot}05$ is required in order to fit the infra-red observations. Although it may be argued that considerable uncertainties yet exist in the interpretation of the infra-red observations, we shall nevertheless adopt $k = 0{\cdot}05$ in the subsequent discussion. In the visible and ultra-violet k may be somewhat less, however. At $\lambda = 2\mu$, $k = 0{\cdot}05$ corresponds to a conductivity

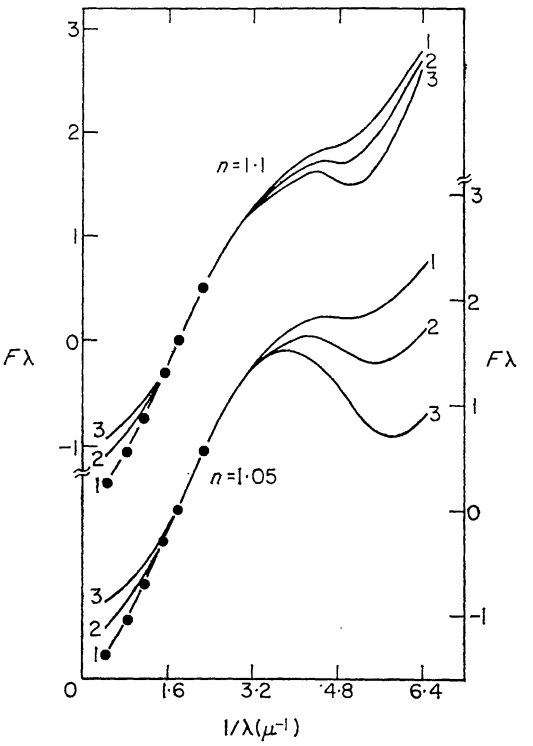

FIG. 4. *Comparison of the theoretical normalized extinction values for a graphite core of radius 0·05 μ surrounded by a solid H_2 mantle of outer radius 0·17 μ with observations (dots) in the red and infra-red region. Curves 1, 2 and 3 refer to cases $k = 0{\cdot}05, 0{\cdot}02$ and 0·00 respectively. The upper and lower sets of curves correspond to $n = 1{\cdot}1$ and 1·05 respectively.*

$\sim 10^{13}\,s^{-1}$, appropriate to a weak semi-conductor. It is likely that impurities and/or radiation damage could produce such a conductivity.

In Fig. 5 we have plotted the normalized extinction caused by graphite cores of radius $r_0 = 0{\cdot}05\mu$ with solid hydrogen mantles of refractive index

$$m = 1{\cdot}05 - 0{\cdot}05i.$$

The several curves (ascending order in figure) correspond to outer mantle radii $r = 0{\cdot}17, 0{\cdot}19, 0{\cdot}21, 0{\cdot}23, 0{\cdot}25\mu$. The points are the observations of Johnson

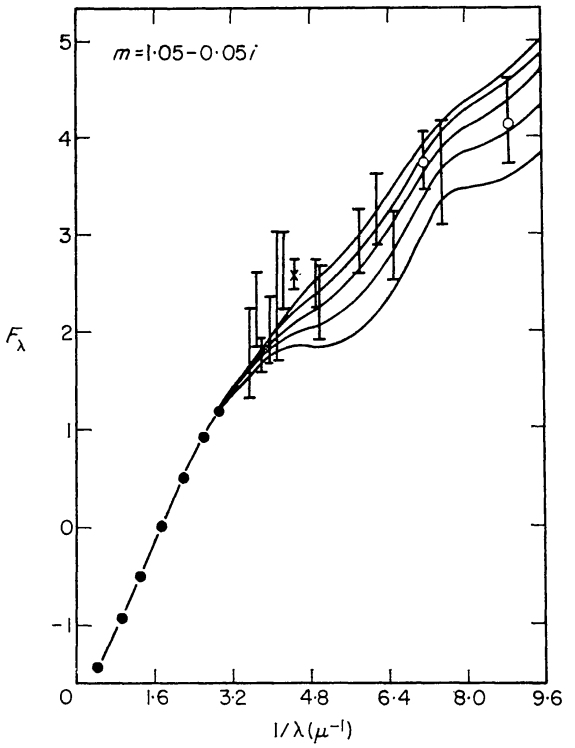

FIG. 5. *Comparison of the theoretical extinction curves for graphite core–solid H_2 mantle particles with observations. Dots denote the mean of the observations of Johnson and Nandy. Bars, cross with bars and circles with bars refer to the observations of Stecher, Boggess & Borgman, and Bless et al. respectively. The theoretical curves are for core radii $r_0 = 0{\cdot}05\ \mu$; the several curves in ascending order in the figure refer to outer mantle radii of $0{\cdot}17\ \mu$, $0{\cdot}19\ \mu$, $0{\cdot}21\ \mu$, $0{\cdot}23\ \mu$ and $0{\cdot}25\ \mu$ respectively. The refractive index of the H_2 mantle is taken to be $m\ (H_2) = 1{\cdot}05 - 0{\cdot}05i$.*

(**33**) in the infra-red, Nandy (**24**) in the visible, Stecher (**22**) and Bless *et al.* (**23**) in the ultra-violet. In Fig. 6 the same quantities are plotted for outer mantles of refractive index $m = 1{\cdot}1 - 0{\cdot}05i$; the core radius is the same as before $r_0 = 0{\cdot}05\mu$ and the outer mantles (in ascending order of curves) are of radii $r = 0{\cdot}15, 0{\cdot}17, 0{\cdot}19, 0{\cdot}21\mu$. The normalized extinction values plotted in Figs 5 and 6 are also set out in Table I.

It is seen from Figs 5 and 6 that very close agreement is possible between the theoretical extinction curves and the observations over a wide range of particle parameters. The stability of the normalized extinction curve over the infra-red and visible spectral region is also quite remarkable. For models with mantle radii in the range $0{\cdot}15$–$0{\cdot}21\ \mu$ represented in Fig. 6, the near ultra-violet variations

do not cover the Cygnus–Perseus difference indicated by Nandy (**24**), (**25**). Either pure graphite particles, or a hydrogen mantle of radius $<0\cdot15\ \mu$ would be required in order to explain the Perseus observations.

The agreement in the ultra-violet includes a slight hump at 2400 Å caused by the graphite cores which persists throughout the theoretical curves. This hump is further accentuated if the absorptive index k in the ultra-violet is somewhat less

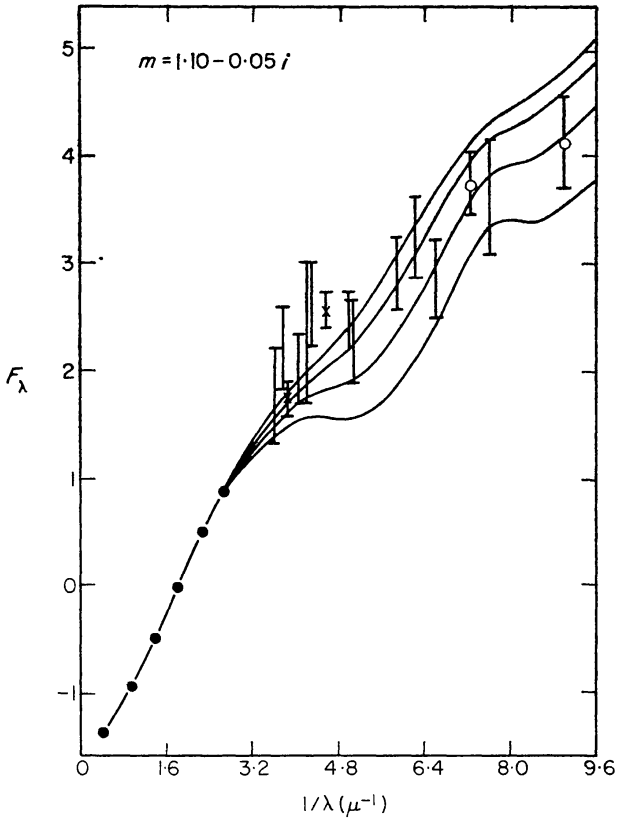

FIG. 6. *Same as Fig.* 5 *except for the following changes: The refractive index of the mantle is taken to be* $m(H_2) = 1\cdot10-0\cdot05i$. *The several curves in ascending order in figure refer to outer mantle radii of* 0·15 μ, 0·17 μ, 0·19 μ *and* 0·21 μ *respectively.*

than 0·05 (see Fig. 4, and Ref. **32**). The theoretical curves also exhibit a second hump in the far ultra-violet at $\lambda^{-1}\sim7\cdot5\ \mu^{-1}$, which is indicated to a slight extent by the observational data. In this context it is also clear that the difference between the cases $n = 1\cdot05$ and $1\cdot10$ is quite insignificant. A further feature that emerged from our calculations is that the present fit with observations, particularly at infra-red and visible wavelengths, is quite insensitive to the precise value of the core radius r_0, provided it is in the range 0·04–0·06 μ.

7. ALBEDO AND PHASE FUNCTION

On the basis of the observations of reflection nebulae and of the diffuse galactic light, it usually claimed that the albedo of grains is high $\gamma>0\cdot5$ and that the scattering diagram is at least moderately forward throwing. The albedo γ and the asymmetry parameter g for the grain models considered in the previous section are set out in Table II, as functions of the wavelength. These quantities are also calculated from the Güttler formulae.

TABLE I

Normalized extinction efficiencies for graphite core–solid hydrogen mantle grains: core radius is 0·05 μ, r stands for outer mantle radius m_{H_2} is solid hydrogen refractive index

$r(\mu)$ / λ^{-1} (μ^{-1})	$m_{H_2} = 1{\cdot}05-0{\cdot}05i$					$m_{H_2} = 1{\cdot}1-0{\cdot}05i$			
	0·17	0·19	0·21	0·23	0·25	0·15	0·17	0·19	0·21
9·68	3·89	4·37	4·70	4·90	5·02	3·83	4·54	4·96	5·14
9·28	3·74	4·21	4·53	4·74	4·85	3·67	4·36	4·79	4·99
8·47	3·53	3·94	4·22	4·41	4·53	3·41	4·02	4·42	4·64
8·07	3·50	3·86	4·12	4·28	4·38	3·41	3·95	4·31	4·50
7·66	3·41	3·75	3·99	4·14	4·24	3·40	3·90	4·22	4·40
7·10	2·96	3·33	3·60	3·79	3·91	3·02	3·56	3·92	4·12
6·61	2·48	2·89	3·19	3·40	3·55	2·48	3·07	3·48	3·74
6·29	2·24	2·64	2·95	3·16	3·32	2·17	2·76	3·18	3·46
5·81	2·01	2·37	2·64	2·84	2·99	1·83	2·37	2·77	3·05
5·49	1·90	2·22	2·47	2·66	2·79	1·68	2·15	2·53	2·80
5·24	1·85	2·13	2·36	2·52	2·65	1·60	2·02	2·36	2·62
4·85	1·84	2·04	2·20	2·34	2·44	1·56	1·87	2·14	2·36
4·40	1·85	1·97	2·06	2·14	2·20	1·60	1·81	1·98	2·11
4·03	1·74	1·83	1·89	1·94	1·98	1·58	1·73	1·85	1·93
3·60	1·51	1·56	1·61	1·64	1·66	1·36	1·47	1·55	1·61
3·23	1·35	1·37	1·38	1·39	1·40	1·23	1·29	1·33	1·36
2·80	1·07	1·07	1·07	1·07	1·06	1·02	1·03	1·05	1·05
2·42	0·70	0·70	0·68	0·70	0·70	0·69	0·69	0·69	0·70
2·24	0·5	0·5	0·5	0·5	0·5	0·5	0·5	0·5	0·5
1·80	0·0	0·0	0·0	0·0	0·0	0·0	0·0	0·0	0·0
1·61	−0·21	−0·21	−0·21	−0·21	−0·21	−0·21	−0·21	−0·21	−0·21
1·45	−0·38	−0·38	−0·39	−0·39	−0·39	−0·39	−0·39	−0·39	−0·39
1·43	−0·41	−0·41	−0·41	−0·42	−0·42	−0·42	−0·41	−0·41	−0·42
1·13	−0·72	−0·73	−0·74	−0·75	−0·76	−0·73	−0·73	−0·73	−0·73
0·97	−0·88	−0·90	−0·91	−0·92	−0·93	−0·87	−0·89	−0·89	−0·89
0·73	−1·12	−1·15	−1·17	−1·19	−1·20	−1·08	−1·11	−1·12	−1·13
0·48	−1·33	−1·37	−1·41	−1·44	−1·46	−1·24	−1·29	−1·32	−1·33

From Table II it is seen that the three cases $m = 1{\cdot}1-0{\cdot}0i$, $m = 1{\cdot}1-0{\cdot}02i$, $m = 1{\cdot}1-0{\cdot}05i$ for the mantle refractive index yield systematically different results. Pure dielectric mantles with $k = 0$ produce high albedos $\gamma > 0{\cdot}5$ and only slightly forward throwing phase functions. The situation for absorptive index $k = 0{\cdot}05$ is that the albedo γ is considerably reduced, but the phase function becomes strongly forward throwing, $g > 0{\cdot}5$.

The precise restriction on the γ, g values of grains is quite uncertain, however. The observations of the diffuse galactic light from below the atmosphere involves several serious sources of error which cannot be completely removed (Wolstencroft & Rose (**34**)). The interpretation of these observations also involve several uncertainties; a detailed radiative transfer model for the galaxy is required before any conclusion concerning γ, g values can be reached.

The most recent observations of the diffuse galactic light (from below the atmosphere) were reported by Witt (**35**). By comparing his observations with the predictions for a plane-parallel slab homogeneous galaxy model, using Eddington's approximation, Witt has concluded that $g = 0$, $\gamma = 1$. This conclusion is highly questionable mainly as a result of uncertainties in the galaxy model employed (**36**)–(**38**). van de Hulst & de Jong (**38**) have subsequently re-interpreted Witt's

TABLE II

Albedos and asymmetry parameters for graphite core–solid hydrogen mantle grains with core radii 0·05

$m(H_2) = 1{\cdot}1 - 0{\cdot}00i$

	$r = 0{\cdot}15\ \mu$		$r = 0{\cdot}17\ \mu$		$r = 0{\cdot}19\ \mu$		$r = 0{\cdot}21\ \mu$	
$\lambda\ (\mu)$	γ	g	γ	g	γ	g	γ	g
0·21	0·64	0·63	0·73	0·74	0·80	0·82	0·87	0·86
0·25	0·70	0·50	0·76	0·60	0·81	0·69	0·85	0·76
0·31	0·60	0·49	0·67	0·57	0·74	0·62	0·79	0·68
0·41	0·54	0·46	0·60	0·58	0·66	0·67	0·72	0·73
0·45	0·53	0·42	0·58	0·55	0·64	0·65	0·70	0·72
0·56	0·49	0·30	0·55	0·42	0·61	0·54	0·68	0·64

$m(H_2) = 1{\cdot}1 - 0{\cdot}02i$

	$r = 0{\cdot}15\ \mu$		$r = 0{\cdot}17\ \mu$		$r = 0{\cdot}19\ \mu$		$r = 0{\cdot}21\ \mu$	
$\lambda\ (\mu)$	γ	g	γ	g	γ	g	γ	g
0·21	0·47	0·69	0·52	0·79	0·56	0·85	0·60	0·89
0·25	0·54	0·58	0·56	0·66	0·58	0·74	0·59	0·80
0·31	0·48	0·57	0·50	0·64	0·53	0·68	0·55	0·73
0·41	0·43	0·50	0·45	0·62	0·47	0·70	0·49	0·76
0·45	0·42	0·45	0·43	0·58	0·45	0·68	0·47	0·75
0·56	0·36	0·32	0·38	0·44	0·40	0·56	0·42	0·65

$m(H_2) = 1{\cdot}1 - 0{\cdot}05i$

	$r = 0{\cdot}15\ \mu$		$r = 0{\cdot}17\ \mu$		$r = 0{\cdot}19\ \mu$		$r = 0{\cdot}21\ \mu$	
$\lambda\ (\mu)$	γ	g	γ	g	γ	g	γ	g
0·21	0·37	0·77	0·40	0·84	0·42	0·89	0·45	0·92
0·25	0·42	0·68	0·42	0·74	0·43	0·80	0·44	0·86
0·31	0·38	0·66	0·39	0·73	0·40	0·76	0·41	0·79
0·41	0·34	0·54	0·34	0·66	0·35	0·74	0·36	0·79
0·45	0·33	0·50	0·33	0·62	0·33	0·71	0·34	0·78
0·56	0·27	0·35	0·28	0·47	0·28	0·59	0·29	0·68

data in terms of a rigorous multiple scattering model of the galaxy and expressed the γ, g requirements at each of two wavelengths ($U = 3597$ Å, $B = 4348$ Å) in terms of loci on the γ, g plane. We have reproduced these loci in Fig. 7. The main uncertainty in the position of these loci arises from uncertainties in Witt's observations which are implied by the wide scatter of his data points (**35**).

The area in Fig. 7 hatched by a single set of parallel lines corresponds to the γ, g values at 3000–4000 Å for the cases with

$$m = \frac{1{\cdot}1}{1{\cdot}05} - 0{\cdot}05i.$$

The cross-hatched domain corresponds to the cases with

$$m = \frac{1{\cdot}1}{1{\cdot}05} - 0{\cdot}02i.$$

The latter cases may be considered more realistic since the impure mantles are expected to be somewhat less absorbing in the blue and ultra-violet than in the red. Within the margin of reliability of the observations, the proximity of the hatched domains to the theoretical loci is quite satisfactory.

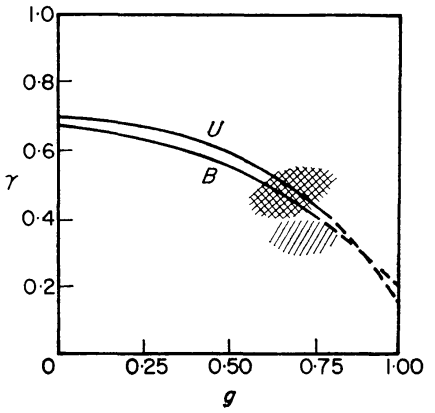

FIG. 7. *Comparison of the calculated values of albedo γ and the asymmetry factor g at 3000–4000 Å for the graphite core–H_2 mantle particles, with observations. The solid curves are van de Hulst and de Jong's representation of the observational data of Witt at U = 3597 Å and B = 4348 Å. The region latched with parallel lines represents the γ, g values for the theoretical models with $m_{H_2} = 1{\cdot}1 - 0{\cdot}05i$; cross-hatched region represents same values for $m_{H_2} = 1{\cdot}1 - 0{\cdot}02i$ (see Table II).*

ACKNOWLEDGMENT

We are grateful to Professor J. van Kranendonk for several communications concerning the properties of solid para-hydrogen. This work was completed while one of us (N.C.W.) held visiting appointments at the Universities of Arizona and Maryland.

Institute of Theoretical Astronomy, University of Cambridge.

K. S. Krishna Swamy*:
NASA Goddard Space Flight Center, Greenbelt, Maryland.

REFERENCES

(1) Wickramasinghe, N. C. & Reddish, V. C., 1968. *Nature, Lond.*, **218**, 661.
(2) Solomon, P. M. & Wickramasinghe, N. C., 1969. *Astrophys. J.*, in press.
(3) Hoyle, F., Wickramasinghe, N. C. & Reddish, V. C., 1968. *Nature, Lond.*, **218**, 1124.
(4) Garzoli, S. L. & Varsavsky, C. M., 1966. *Astrophys. J.*, **145**, 79.
(5) Kerr, F. J. & Garzoli, S., 1968. *Astrophys. J.*, **152**, 51.
(6) Reddish, V. C., 1967. *Mon. Not. R. astr. Soc.*, **135**, 251.
(7) Reddish, V. C. & Wickramasinghe, N. C., 1969. *Mon. Not. R. astr. Soc.*, **143**, 189.
(8) Reddish, V. C., 1968. *Q. Jl. R. astr. Soc.*, **9**, 409.
(9) Hayakawa, S., 1968. Personal communication.
(10) Hoyle, F. & Wickramasinghe, N. C., 1967. *Nature, Lond.*, **214**, 969.
(11) Sears, V. F. & van Kranendonk, J., 1964. *Can. J. Phys.*, **42**, 980.
(12) van Kranendonk, J., 1968. Personal communication.
(13) Lynds, B. T. & Wickramasinghe, N. C., 1968. *Ann. Rev. Astr. Astrophys.*, **6**, 215.
(14) Wickramasinghe, N. C. & Williams, D. A., 1968. *Observatory*, **88**, 272.
(15) Skinner, G. B. & Ringrose, G. H., 1965. *J. chem. Phys.*, **42**, 2190.
(16) Carroll, T. O. & Salpeter, E. E., 1966. *Astrophys. J.*, **143**, 609.
(17) Stewart, J. W., 1964. *J. chem. Phys.*, **40**, 3297.
(18) Mills, R. L. & Schuch, A. F., 1965. *Phys. Rev. Lett.*, **15**, 722.
(19) Taft, E. A. & Phillipp, H. R., 1965. *Phys. Rev.*, **138A**, 197.

* NAS-NRC postdoctoral research associate.

(20) Taft, E. A. & Phillipp, H. R., 1967. Personal communication of computer print-outs.
(21) Boggess, A. & Borgman, J., 1964. *Astrophys. J.*, **140**, 1636.
(22) Stecher, T. P., 1965. *Astrophys. J.*, **142**, 1683.
(23) Bless, R. C., Code, A. D. & Houk, T. E., 1968. *Astrophys. J.*, **153**, 561.
(24) Nandy, K., 1964. *Publs R. Obs. Edinb.*, **3**, No. 6.
(25) Nandy, K., 1965. *Publs R. Obs. Edinb.*, **5**, 13.
(26) Wickramasinghe, N. C., 1967. *Interstellar Grains*, Chapman & Hall, London.
(27) Field, G. B., Partridge, R. B. & Sobel, H., 1967. In *Interstellar Grains*, ed. by J. M. Greenberg and T. P. Roark, NASA SP-140, Washington.
(28) Donn, B. & Krishna Swamy, K. S., 1969. *Physica*, **41**, 144
(29) Danielson, R. E., Woolf, N. J. & Ganstad, J. E., 1965. *Astrophys. J.*, **141**, 116.
(30) Cudaback, D. D., Ganstad, J. E. & Knacke, R. J., 1969. Preprint.
(31) Krishna Swamy, K. S. & Wickramasinghe, N. C., 1969. *Observatory*, **89**, 57.
(32) Wickramasinghe, N. C. & Nandy, K., 1968. *Nature, Lond.*, **219**, 1347.
(33) Johnson, H. L., 1965. *Astrophys. J.*, **141**, 923.
(34) Wolstencroft, R. D. & Rose, L. J., 1966. *Nature, Lond.*, **209**, 389.
(35) Witt, A. N., 1968. *Astrophys. J.*, **152**, 59.
(36) Wickramasinghe, N. C., 1968. *Nature, Lond.*, **218**, 1039.
(37) Wickramasinghe, N. C. & Wolstencroft, R. D. In preparation.
(38) van de Hulst, H. C. & de Jong, T., 1969. *Physica*, **41**, 151.
(39) Brackmann, R. T. & Fite, W. L., 1961. *J. chem. Phys.*, **34**, 1572.
(40) Bok, B. J., 1956. *Astr. J.*, **61**, 309.